Annu. Rev. Fluid. Mech. 1997. 29:245–83

PARABOLIZED STABILITY EQUATIONS

Thorwald Herbert
DynaFlow, Inc, Columbus, Ohio 43221-0319, and Department of Mechanical Engineering, The Ohio State University, Columbus, Ohio 43210-1107;
e-mail: Herbert@dynaflow.com

KEY WORDS: boundary-layer stability, laminar-turbulent transition, laminar flow control

ABSTRACT

Parabolized stability equations (PSE) have opened new avenues to the analysis of the streamwise growth of linear and nonlinear disturbances in slowly varying shear flows such as boundary layers, jets, and far wakes. Growth mechanisms include both algebraic transient growth and exponential growth through primary and higher instabilities. In contrast to the eigensolutions of traditional linear stability equations, PSE solutions incorporate inhomogeneous initial and boundary conditions as do numerical solutions of the Navier-Stokes equations, but they can be obtained at modest computational expense. PSE codes have developed into a convenient tool to analyze basic mechanisms in boundary-layer flows. The most important area of application, however, is the use of the PSE approach for transition analysis in aerodynamic design. Together with the adjoint linear problem, PSE methods promise improved design capabilities for laminar flow control systems.

INTRODUCTION

Before we discuss parabolized stability equations, it is useful to review the relationship between stability and transition in viscous shear flows. The subject starts with the work of Reynolds (1883), who studied the variation of the flow rate of water through circular pipes and reported observations of fundamental importance to the work of generations of engineers and scientists. The smooth variation of the flow rate with the pressure gradient exhibited a remarkable break at a fixed value of the parameter $\bar{V}D/\nu \approx 3000$, where $\bar{V}$ is the average velocity, D is the pipe diameter, and ν is the kinematic viscosity. Reynolds

0066-4189/97/0115-0245$08.00

found the break to be caused by the transition from *laminar* to sinuous or *turbulent* motion and related this transition to an instability of the laminar flow. Orr (1907) and Sommerfeld (1908), who also named the critical parameter the *Reynolds number*, independently derived the equations for the analysis of small disturbances in viscous parallel flows but were unable to find instability. This result was not surprising because the flows studied are stable in the absence of viscosity, and the anticipation of a destabilizing effect of viscosity (Prandtl 1921, 1922) is counterintuitive. Nevertheless, Tollmien (1929) succeeded in solving the Orr-Sommerfeld problem for the Blasius boundary-layer flow and for the first time, calculated a neutral curve that encloses the region of instability and the critical value Re^*_{cr} below which the laminar flow is stable. The Reynolds number $Re^* = U_\infty \delta^*/\nu$ is formed with the freestream speed U_∞ and displacement thickness δ^*. The growth of the boundary-layer thickness was neglected in this analysis by the assumption of a *locally parallel flow* to meet the prerequisites of the theory.

The solutions of the Orr-Sommerfeld problem have the general form $v' = v(y)\exp[i(\alpha x + \beta z - \omega t)]$, where x, y, and z are coordinates streamwise, normal to the wall, and spanwise, respectively. The wavenumbers α of the unstable disturbance waves are much smaller than those of turbulent fluctuations, and the growth rates ω_i calculated by Schlichting (1933) are feeble owing to the viscous origin of the instability. The critical Reynolds number Re^*_{cr} is significantly lower than the value of Re^*_{tr} where transition occurs in experiments. Squire (1933) showed furthermore that the instability problem for three-dimensional (3D) disturbances with $\beta \neq 0$ can be reduced to an equivalent two-dimensional (2D) problem at a lower Reynolds number. Hence the onset of instability is associated with 2D waves while turbulent fluctuations are 3D. Strong objections to the relevance of the linear instability theory to transition (Taylor 1938) were not overcome until Schubauer & Skramstad (1943, 1947) found the predicted waves experimentally. Liepmann (1943), aware of the then classified findings, apparently was the first to convert linear stability results into a transition criterion for practical applications.

Transition Prediction

Liepmann's criterion is based on the ratio A/A_0, where $A = A(x)$ is the wave amplitude as it evolves downstream, and A_0 is the unknown but small amplitude at the onset position x_0 of instability. Calculation of this amplitude ratio required obtaining the complex frequency $\omega = \omega_r + i\omega_i$ for waves of different wavenumbers α for the changing local boundary-layer profiles along the body, and integration of the small spatial growth rates ω_i/c over a considerable distance in x. Gaster (1962) showed that the phase velocity c must be replaced by the group velocity c_g to correctly convert the temporal to the spatial growth

rate. His study also suggested solving the Orr-Sommerfeld problem for real frequencies $\omega = \omega_r$ to obtain the spatial growth rate $-\alpha_i$ directly from the complex wavenumber $\alpha = \alpha_r + i\alpha_i$. The amplitude ratio then is given by

$$\sigma(x;\omega) = \ln\left(\frac{A}{A_0}\right) = -\int_{x_0}^{x} \alpha_i(\xi;\omega)d\xi. \quad (1)$$

Liepmann related the critical value of the amplitude ratio to the skin-friction coefficient C_f in laminar flow. Smith & Gamberoni (1956) and Van Ingen (1956) later found independent of each other that transition in wind-tunnel tests of airfoils correlated well with values of the *N factor*

$$N = \max_{\omega} \sigma(x_{tr};\omega) \quad (2)$$

between 7 and 9. This observation is the basis of the e^N method of transition prediction that links the transition location to a certain degree of amplification: $A_{tr}/A_0 \approx e^N$. The e^N method for 2D TS waves[1] has been extended to compressible and 3D boundary layers, and to other types of instability such as Görtler vortices (Görtler 1940) on concave walls, crossflow instability in 3D flows over infinite swept wings (Gray 1952, Gregory et al 1955), and Mack's higher modes in supersonic flows (Mack 1969). Today the e^N method is the mainstay of transition prediction in aerodynamic design, and many millions of dollars have been spent gathering each of the "golden data points" needed for the empirical correlations in flight tests, because wind-tunnel data are biased by the different disturbance environment. In the design of commercial aircraft, this cost is justified by the dramatic reduction of drag achieved by a shift of the transition location downstream. The significant change in drag with x_{tr} is caused by the large disparity of the skin friction in laminar and turbulent flow, and an accurate prediction of x_{tr} becomes of foremost importance for reliable estimates of the drag. Arnal (1984, 1994) and others have surveyed the status of this field, Mack (1984) has presented the underlying linear stability theory for boundary layers, and Reed et al (1996) have evaluated more recent results.

Nonlinear Effects

The e^N method often has been criticized because it can account neither for the known influence of the disturbance level nor for the nonlinear mechanisms that cause changes of the mean flow and skin-friction coefficient as well as the breakdown of the laminar flow. Experiments of Klebanoff et al (1962) revealed that the growth of TS waves indeed continues over a large distance downstream of x_0. As the amplitude (measured as the maximum streamwise rms fluctuation $u'_{\max}$) exceeds about 1% of the freestream velocity U_∞, the waves

[1]TS stands for Tollmien, Schlichting, Schubauer, and Skramstad.

exhibit a rapidly growing spanwise periodic variation and a simultaneous growth of longitudinal vortices. Breakdown of the flow occurs quickly thereafter as the peak amplitudes exceed about 10%. The breakdown or transition location clearly varies with the initial amplitude of the TS wave. The spanwise variation is governed by low-frequency Klebanoff modes (Klebanoff 1971) that appear in many experiments as a slowly growing ($A \sim x^{1/2}$) instability that is outside of the exponential growth concept of the linear stability theory (LST). A different type of transition has been observed by Kachanov & Levchenko (1984, see also Kachanov 1994) at even smaller levels of the TS amplitude. The dominant feature in this case is the rapid growth of spanwise periodic subharmonic waves.

The growth of spanwise periodic disturbances on a fast vortical scale has been explained by the Floquet theory of secondary instability (Herbert 1988). In a Galilean frame moving with the phase speed c, boundary-layer flow and finite-amplitude TS wave form a new flow that is nearly periodic in $x' = x - ct$. This flow is subject to various types of parametric instabilities if the wave amplitude exceeds the associated thresholds to overcome the damping of the viscous system. Subharmonic resonance occurs at lower amplitudes than the fundamental parametric instability that Klebanoff observed.

Direct numerical simulations (DNS) have revealed transition evolving from the nonlinear interaction of oblique waves in a 2D supersonic boundary layer without participation of a secondary instability (Fasel et al 1991, 1993). The catalog of nonlinear mechanisms in aerodynamic boundary layers is still incomplete.

Nonparallel Effects

Besides nonlinearity, streamwise variations of the boundary layers may affect the accuracy of the growth rates used in the e^N method. Even small deviations may accumulate during the integration over a large streamwise distance. Although carried out with utmost care, theoretical and experimental results for Blasius flow show significant differences in the neutral curves.

Since the nonparallel effects are of the small order $\mathcal{O}(Re^{-1})$, where $Re = Re_x^{1/2}$, $Re_x = U_\infty x/\nu$, perturbation methods were employed by Bouthier (1972, 1973), Gaster (1974), and Saric & Nayfeh (1977) to obtain corrected results for 2D waves in Blasius flow. Though based on similar concepts, the formulations are different, and so are the results. Saric & Nayfeh's results were generally accepted and supported by the experimental data of Kachanov et al (1975) but are today known to be in error. Bouthier's results are difficult to compare with experiments. Gaster obtained a result unexpectedly similar to the neutral curve for parallel flow and excluded nonparallelism as the cause of the deviations between theory and experiment.

In an effort to clarify the situation and to obtain results for 3D disturbances, this author critically repeated the steps of the analysis. Use of the WKBJ approximation or multiple scales provides at some intermediate step a partial differential equation similar to the parabolized Navier-Stokes equations, except for additional terms containing frequency and wavenumbers. Gaster has mentioned the parabolic character of closely related equations; however, previous analyses proceeded to reduce the problem further, to more tractable ordinary differential equations. These final steps are not only unnecessary but severely restrict the scope and validity of the resulting equations. The intermediate partial differential equations, which we named *parabolized stability equations* or *PSE* for short, can be solved directly by a marching procedure. Herbert & Bertolotti's (1987) initial results confirmed Gaster's results and encouraged exploring the potential of the PSE for research and engineering applications. The following discussion surveys the results.

DISTURBANCE AND STABILITY EQUATIONS

For simplicity we illustrate the PSE concept for an incompressible flow that satisfies the linear continuity equation and nonlinear momentum equations

$$\nabla\hat{\mathbf{v}} = 0,\ \frac{\partial\hat{\mathbf{v}}}{\partial t} - \frac{1}{Re}\nabla^2\hat{\mathbf{v}} + (\hat{\mathbf{v}}\cdot\nabla)\hat{\mathbf{v}} + \nabla\hat{p} = 0, \tag{3}$$

where $\hat{\mathbf{v}}$ is the velocity vector, $\hat{p}$ is the pressure, and $Re = Re_x^{1/2}$, $Re_x = U_\infty x/\nu$, the Reynolds number. As is common for stability analysis, we decompose the total flow field by $\hat{\mathbf{v}} = \mathbf{V} + \mathbf{v}'$, $\hat{p} = P + p'$ into the steady laminar basic flow $\mathbf{V}$, P, and the disturbance $\mathbf{v}'$, p'. Provided the basic flow is a known solution of Equations 3 under given boundary conditions, substitution leads to the nonlinear *disturbance equations*

$$\nabla\mathbf{v}' = 0,\ \frac{\partial\mathbf{v}'}{\partial t} - \frac{1}{Re}\nabla^2\mathbf{v}' + (\mathbf{v}'\cdot\nabla)\mathbf{V} + (\mathbf{V}\cdot\nabla)\mathbf{v}' + \nabla p' = (\mathbf{v}'\cdot\nabla)\mathbf{v}'. \tag{4}$$

These equations are as exact as Equations 3. The nonlinear term on the right can be neglected for sufficiently small disturbances. The coefficients of the resulting linear disturbance equations are determined by the basic velocity $\mathbf{V}$ and show the same dependencies on the spatial variables. The boundary conditions are usually homogeneous but may contain small disturbances that leave the basic flow unaffected.

Linear Stability Equations

In Cartesian coordinates x, y, z, we use the velocity components $\mathbf{v}' = (u', v', w')$. The traditional LST exploits the properties of the linear disturbance equations

for parallel flows, $\mathbf{V} = [U(y), 0, W(y)]$. In this case, the disturbances can be written as *normal modes*

$$\mathbf{q}'(x, y, z, t) = \mathbf{q}(y) \exp[i(\alpha x + \beta z - \omega t)], \tag{5}$$

where $\mathbf{q}' = [u', v', w', p']^T$ is the vector of flow variables and $\mathbf{q} = [u, v, w, p]^T$ is the vector of the associated shape functions. The exponential factor with wavenumbers α and β in x and z, respectively, and frequency ω describes the wave nature of the solution. Introducing the normal modes (Equation 5) into the linear disturbance equations yields the normal-mode or *stability equations*, which in compact form can be written as an eigenvalue problem

$$L\mathbf{q} = 0, \tag{6}$$

with homogeneous boundary conditions on u, v, w. The operator L contains differentiation in y only. After proper manipulation, L can assume different forms, for example, the form of the Orr-Sommerfeld and Squire equations.

For given U and W, the eigenvalue problem can be reduced to solving a complex characteristic equation of the form

$$\mathcal{F}(Re, \alpha, \beta, \omega) = 0, \tag{7}$$

which yields two quantities per eigenmode, provided that all other parameters are given. For boundary layers, it is most appropriate to specify the real quantities Re, β, and ω and determine $\alpha = \alpha_r + i\alpha_i$ from Equation 7 to obtain the spatial growth rate $-\alpha_i$ in the x direction. Unfortunately, different powers of α appear in the equations and cause difficulty for many eigenvalue solvers. Therefore, the problem is often solved for the eigenvalue ω with real Re, α, and β to obtain the temporal growth rate ω_i. The spatial growth rate for the integral in Equation 1 is approximated by Gaster's transformation $\alpha_i \approx -\omega_i / c_g$.

Parabolized Stability Equations

Boundary layers are in general not parallel. The velocity components U and W exhibit small variations in the streamwise and spanwise direction, and the component V normal to the surface is non-zero to provide the mass balance as the displacement thickness δ^* changes. Let us introduce the small parameter $\epsilon = \mathcal{O}(Re^{-1})$ and the slowly varying variables $\xi = \epsilon x$, $\zeta = \epsilon z$. Then we can write the basic flow in the form $\mathbf{V} = [U(\xi, y, \zeta), \epsilon V(\xi, y, \zeta), W(\xi, y, \zeta)]$. For this flow the Navier-Stokes equations reduce at order $\mathcal{O}(\epsilon)$ to Prandtl's boundary-layer equations.

For the disturbances $\mathbf{q}'(x, y, z, t)$ we cannot enforce a similar form because $v' = \mathcal{O}(u')$ and the wavenumbers are not small. However, we can adapt the

concept of normal modes that leads initially to

$$\mathbf{q}'(x, y, z, t) = \tilde{\mathbf{q}}(x, y, z, t) \exp[i\tilde{\theta}(x, z, t)], \tag{8}$$

with a phase function $\tilde{\theta}$.

A slow variation of $\tilde{\mathbf{q}}$ in x, z may not be assumed, because oscillations and growth in x and z can be absorbed into $\tilde{\mathbf{q}}$ as well as the phase function $\tilde{\theta}$. This ambiguity must be removed by conditions on the variation of $\tilde{\mathbf{q}}$ with x and z. Ideally we would like $\tilde{\mathbf{q}}$ to be independent of x and z. This desirable property can only be achieved locally or in some average sense across the domain Ω in y. In the simple case of a 2D wave in 2D flow, one can apply a local norm such as $|u(y^*)| = const.$ at some suitable distance y^* from the wall. In more general cases, we prefer integral norms that are both physically and mathematically meaningful,

$$\int_\Omega \mathbf{v}^\dagger \frac{\partial \mathbf{v}}{\partial \xi} dy = 0, \int_\Omega \mathbf{v}^\dagger \frac{\partial \mathbf{v}}{\partial \zeta} dy = 0, \tag{9a,b}$$

where the dagger denotes the complex conjugate. This choice makes the total kinetic energy $\int_\Omega |\mathbf{v}|^2 dy$ of the shape functions independent of ξ and ζ. The growth of the disturbance energy is absorbed into the phase function θ, and the growth rate $-2\theta_i$ refers directly to the total kinetic energy $\int_\Omega |\mathbf{v}'|^2 dy$ of the disturbance. Under the conditions 9a and 9b, we can write

$$\mathbf{q}'(x, y, z, t) = \mathbf{q}(\xi, y, \zeta, t) \exp[i\theta(x, z, t)] \tag{10}$$

with slowly varying shape functions and a well-defined phase function θ. Moreover, we obtain

$$\omega = \frac{\partial \theta}{\partial t}, \ \mathbf{k}(\xi, \zeta) = (\alpha, \beta) = \nabla\theta \tag{11}$$

with a slowly varying wavenumber vector $\mathbf{k}$ in the x, z plane. Since $\nabla \times \nabla\varphi = 0$ for any scalar function φ, the wavenumbers must satisfy the irrotationality condition (Mack 1977)

$$\nabla \times \mathbf{k} = 0, \ \frac{\partial \alpha}{\partial \zeta} = \frac{\partial \beta}{\partial \xi}, \tag{12a,b}$$

where Equation 12b can also be derived from the Cauchy-Riemann equations. Substitution of Equations 10 and 11 into the nonlinear disturbance Equations 4 yields up to $\mathcal{O}(\epsilon)$ the parabolized stability equations

$$(L + \epsilon L')\mathbf{q} + \epsilon M_1 \frac{\partial \mathbf{q}}{\partial \xi} + \epsilon M_2 \frac{\partial \mathbf{q}}{\partial \zeta} = \mathbf{r} - \epsilon \left[\frac{d\alpha}{d\xi} N_1 \mathbf{q} + \frac{d\beta}{d\zeta} N_1 \mathbf{q} \right], \tag{13}$$

where the operators L, L', M_1, M_2, N_1, N_2 act in y only.[2] The term in square brackets can be neglected because N_1 and N_2 originate from the viscous terms and are of $\mathcal{O}(Re^{-1})$. The function $\mathbf{r} = \mathbf{r}(y)$ on the right-hand side represents nonlinear terms that need further discussion below. The operator L' contains the nonparallel contributions V, $\partial U/\partial\xi$, ... of the basic flow. After linearization, the limit $\epsilon \to 0$ retrieves the governing Equation 6 of the LST.

SPECIAL CASES For basic flows independent of the spanwise direction z, the PSE assume the simple form

$$(L + \epsilon L')\mathbf{q} + \epsilon M_1 \frac{\partial \mathbf{q}}{\partial \xi} = \mathbf{r} \tag{14}$$

and only one norm (Equation 9a) is needed. The irrotationality condition leads to a constant value of β for $\alpha = \alpha(\xi)$. This form of the PSE governs parallel flows, where $L' \equiv 0$, 2D flows, and the quasi-3D flows on swept cylindrical bodies such as infinite swept wings. This special case has been studied in detail by Bertolotti (1991) and is the basis of virtually all PSE applications. For $\alpha = 0$, the PSE are closely related to the parabolic equations introduced by Hall (1983) for the analysis of Görtler vortices.

The solution requires both initial and boundary conditions. To model the situation considered by the LST, we assume homogeneous boundary conditions on $\mathbf{v}$ in y. As an initial condition we can specify some solution provided by the LST at a starting position x_s. The coupled Equations 14 and 9a can then be solved by a marching procedure for $x > x_s$ while keeping β constant. The norm serves to update the value of α at every marching step.

EARLY RESULTS Initial results of the linear problem ($\mathbf{r} = 0$) for 2D waves in the Blasius boundary layer were presented a few months after conception of the PSE (Herbert & Bertolotti 1987). Figure 1 shows a later comparison of LST, PSE, and DNS results. The nonparallel effects at this frequency $F = \omega/Re = 50 \cdot 10^6$ are relatively small, and we find perfect agreement between PSE and DNS results for the variation of $u'_{\max}$ with Re. The figure also shows another effect of nonparallelism. In the LST all quantities grow at the same rate. In nonparallel flows the growth rate depends on how the amplitude is measured (Bouthier 1972). Therefore, the use of the integral kinetic energy provides a different growth curve, although the physical solution is the same. In nonparallel flows, the N factor demands a more precise definition.

Figure 2 compares the neutral curves for parallel and nonparallel flow and confirms Gaster's results. The nonparallel effects on 2D waves are in fact small and decrease with the frequency F. The discrepancy between experimental

[2]The detailed form of the operators for spanwise uniform flows is given by Herbert (1994).

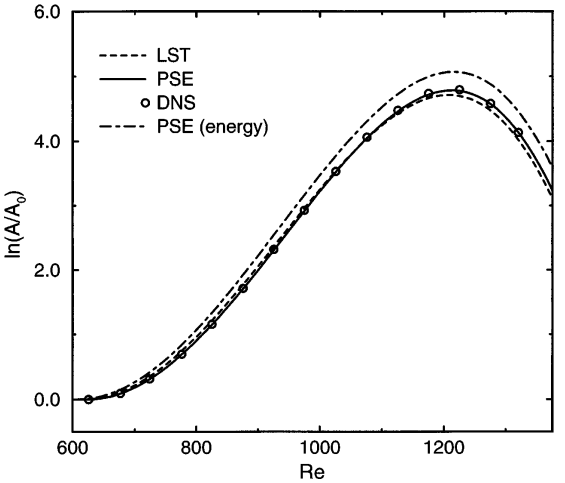

Figure 1 Amplitude growth curves based on u'_{max} and the integral kinetic energy for $F = 50 \cdot 10^6$. Comparison of LST, PSE, and DNS. (Data of Bertolotti et al 1992.)

and theoretical results is not caused by the nonparallelism of the Blasius flow (nor is it caused by nonlinear effects, but likely by slight pressure gradients, see Bertolotti et al 1992). After the confirmation of Gaster's results, Saric (1989) has discussed numerous sources of experimental error and has proposed remedies.

While the 2D results indicate a small effect of nonparallelism, the growth of 3D disturbances is significantly different, as shown by the results of the LST and PSE in Figure 3.

With these results, we clarified the answers to the original questions that led to the PSE approach. This success has encouraged ongoing efforts to analyze this approach in more detail and to explore its full potential.

VALIDITY OF THE PSE The use of a marching technique for solving the PSE is permitted only if the stability problem is governed by downstream propagating information. According to their propagation characteristics, we can distinguish absolute and convective instabilities (Huerre & Monkewitz 1990). In these terms the PSE approach is valid for convectively unstable flows. This class contains pipe and channel flows; entrance flows; and the technologically important boundary layers, mixing layers, far wakes, and others that make it worthwhile pursuing this new avenue.

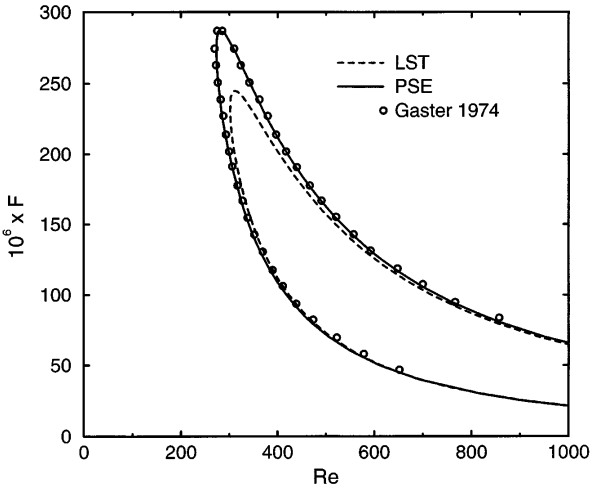

Figure 2 The neutral curves of the LST and for nonparallel flow according to PSE and Gaster (1974). (Data of Bertolotti et al 1992.)

The convective nature of linear instabilities can be assured by analysis. For nonlinear problems we must rely on experience and comparison with experimental or other computational results.

PARABOLIZED VS PARABOLIC Are the PSE really parabolic? The negative answer can easily be found by marching with a sufficiently small step size, which leads to strong numerical instability. Similar to the parabolized Navier-Stokes equations (PNS), the PSE exhibit weak ellipticity. Haj-Hariri (1994) performed a characteristics analysis of the PSE system that shows weak ellipticity of acoustic origin for $\alpha \neq 0$. He suggests neglecting one of the responsible small terms ($\partial p/\partial x$ in the x-momentum equation) to alleviate this effect; however, this measure has limited influence. An alternative is to choose a sufficiently large marching step to "skip" over the small upstream influence, which also increases the method's efficiency in practical applications. For marching with simple backward differences, Li & Malik (1994) obtained the limit $\Delta x > |\alpha|^{-1}$ for the marching step Δx. Although this limit is acceptable for most applications, it prevents resolving rapid variation of the shape functions, for example, in the late stages of transition, which may also violate the key assumption underlying the PSE method.

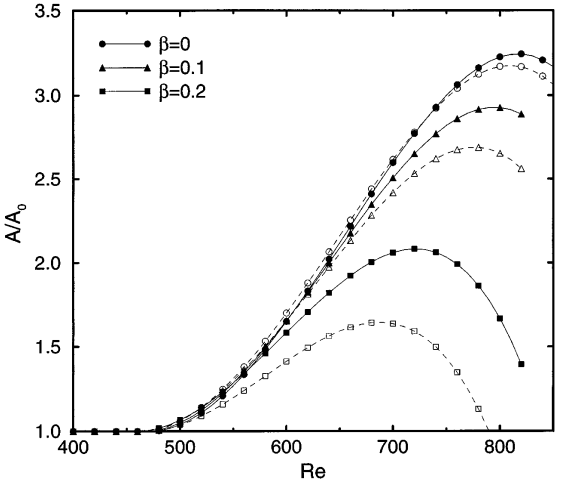

Figure 3 Growth rates for modes with $F = 86 \cdot 10^6$ and different wavenumbers $\beta = \beta^* \nu / U_\infty$ according to PSE (*full symbols*) and LST (*open symbols*). (Data of Bertolotti 1991.)

Studies on the mathematical nature of the PSE (Equation 14) have neglected so far the need for a norm [(Equation 9) or any of the numerous alternatives listed by Airiau (1994)], and do not consider the close relationship between the operators (e.g. $M_1 = -i\partial L/\partial\alpha$). In the hands of an applied mathematician the PSE approach can probably be improved beyond its current capabilities.

Advantages of the PSE

PSE VS LST The PSE account for the history of the disturbance and for the streamwise variation of the basic flow. Nonparallelism is partially included even if $L' \equiv 0$. The operator L' requires small-velocity terms that are not provided by most boundary-layer codes and are difficult to retrieve from numerical data. The PSE provide a connected physical solution along the marching path and the spatial amplitude growth curves $\sigma(x; \omega, \beta)$ directly for use in the e^N method. Long waves and surface curvature can be treated consistently. The initial-boundary-value problem is suitable for analyzing exponential as well as transient growth of disturbances. The PSE can be solved with disturbed boundary conditions. These inhomogeneous conditions include freestream turbulence or roughness that do not affect the basic flow. The PSE allow for an inhomogeneous right-hand side $\mathbf{r}$ that may originate from the nonlinear terms

$(\mathbf{v}' \cdot \nabla)\mathbf{v}'$) in Equations 4, in combination with other forcing functions. Systems of PSE for different frequencies ω_n and wavenumbers β_m can be solved simultaneously to trace the nonlinear evolution of single modes or the interaction of different modes. For these reasons, the PSE approach is suitable for simulating the early stages of transition.

PSE VS DNS The PSE have been extended to compressible flows (Bertolotti & Herbert 1991) and general curvilinear coordinates (Herbert et al 1993b). The solutions do not suffer from large ratios of the disturbance amplitude ($e^{10} \approx 22,000$) in different regions of the computational domain, as do DNS solutions. There is no need to deal with nonintrusive outflow conditions. With a restricted number of modes, the PSE method allows fast transition simulations up to the breakdown stage where significant changes in the skin friction (or heat transfer) occur. The marching procedure terminates typically because the iterative update of the wavenumber or the iterative solution of the nonlinear system for different modes fails to converge.

AREAS OF APPLICATION The PSE complement, rather than compete with, DNS. Systematic research on nonlinear processes and transition can be performed at low cost on practically any computer from a 90-MHz 486 laptop up. This makes engineering design a prime area for PSE applications. Linear PSE codes provide reliable amplitude-growth curves for the e^N method. Use of nonlinear analysis permits improved transition predictions by accounting for different disturbance levels in free flight, wind tunnels, or gas turbines. Since Herbert (1991) has discussed these opportunities and unresolved issues, slow but steady progress has been made toward developing PSE-based design tools.

Following an internal report by Bertolotti (1989), the PSE approach has been embraced at NASA Langley (Chang et al 1991) and subsequently at ONERA/CERT Toulouse (Airiau & Casalis 1994), FFA Stockholm, and DLR Göttingen (Simen et al 1994) for the analysis of boundary layers on realistic geometries. Some efforts at DLR use a *nonlocal instability theory* developed by Simen (1992). Even though this approach starts from a broader background, the equations solved seem to be identical with the PSE. Although the numerical treatment varies, the published results do not indicate any progress over the original PSE formulation.

FLOWS OVER FLAT PLATES

So far we have stated benefits of the parabolized stability equations without providing proof. In this section we demonstrate some of the capabilities for flows over flat plates. Incompressible flow in a zero-pressure gradient is often chosen as a benchmark because the basic flow and stability characteristics are

well known, and data for comparison are available from experiments and DNS. There are unresolved issues, however, even in this virtually simple case.

HARMONIC POINT SOURCE Natural sources rarely produce single instability modes but rather wave motions with broad wavenumber spectra. A weak harmonic point source is the simplest model that produces a broad spectrum of spanwise wavenumbers β at a single frequency ω, and its influence on the flow has been studied in various experiments. Mack & Kendall (1983) found the growth along the centerline calculated using LST with a uniform initial spectrum to be well above the measured data, an observation Gaster (1975) made earlier for a pulsed point source. The disagreement was attributed to nonparallel effects.

Mack & Herbert (1995) repeated the analysis with a linear PSE run using a uniform initial spectrum of up to 211 modes. Figure 4 shows the resulting wave pattern created by a harmonic point source at $x_s = 475$ with frequency $F = 60 \cdot 10^{-6}$, where the reference length is $\delta_r = (\nu x/U_\infty)^{1/2}$. The initial disturbance is given by modes with equal initial $u'_{\max}$ amplitudes and phases and $\beta_m = 0.0075 \cdot m$, $m = 0, \ldots, 200$. While the spanwise location of the peak amplitude is in agreement with the experiment, the growth of the centerline amplitude is close to the LST result and data of Balakumar & Malik (1992) obtained with a nonuniform initial spectrum and a local nonparallel theory. DNS runs show strong dependence of the near-field of the source on the source geometry. This near-field cannot be captured by LST or PSE. However, the discrepancy between measured and calculated data further downstream must be sought in deviations of the experiments from the computational model, as discussed by Saric (1989).

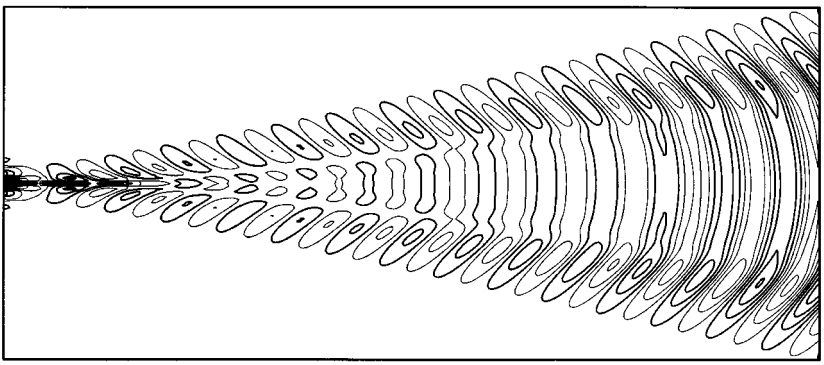

Figure 4 Waves created by a harmonic point source. Contours of equal streamwise disturbance velocity for $0 \le x - x_s \le 1000$ at $y = 2.5$.

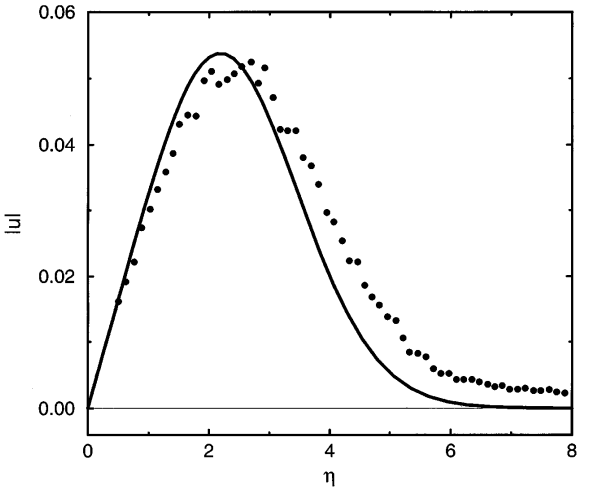

Figure 5 Velocity distribution of the steady Klebanoff mode at $Re = 717$. Comparison with experimental data of Kendall (1990).

KLEBANOFF MODES Low-frequency disturbances cause a streaky modulation of the boundary-layer flow in many, if not all, wind-tunnel experiments owing to residual streamwise vorticity produced by the screens and enhanced by the contraction into the test section. Herbert & Lin (1993) have investigated a related problem in which low-frequency spanwise periodic nonuniformities are introduced, for example, by nonuniform suction. While the average suction level affects the basic flow, small disturbances cause inhomogeneous boundary conditions for the PSE solution. The amplitudes of the disturbances introduced at some starting position x_s indeed grow initially to large values and ultimately decay. The shape functions show the characteristics reported by Kendall (1990), as in Figure 5, and the amplitudes for different frequencies are consistent with the spectra measured by Klebanoff. Some differences are likely to reflect the effect of a distributed excitation in the experiment vs the local excitation in the PSE study.

The results on Klebanoff modes are a spatial version of the transient temporal growth mechanism analyzed by Butler & Farrell (1992). The issue of transient growth of disturbances in shear flows has been clarified by Schmid & Henningson (1992), Reddy & Henningson (1993), and Trefethen et al (1993). Waleffe (1995) has given an illustrative example of the transient growth evolving from the interaction of two stable modes of the Orr-Sommerfeld equation

and Squire equation, respectively. Klebanoff (1971) was in fact correct when he attributed the growth of low-frequency modes to an independent—though not exponential—instability of the boundary layer. TS modes and Klebanoff modes coexist at the same spanwise wavenumber and frequency but hardly interact because the unsteady Klebanoff modes travel at a higher phase speed.

The growth of low-frequency Klebanoff modes is weaker on convex walls and leads to unstable Görtler vortices on concave walls. The same mechanism causes the subcritical growth of crossflow vortices in the Hiemenz flow on a swept plate, where the excitation can be attributed to nonuniform roughness or suction.

Bertolotti (1996) used the PSE method to analyze the response of the Blasius flow to freestream vorticity, especially longitudinal vorticity. He found the growth for the most amplified spanwise wavenumbers and velocity distributions of the generated Klebanoff modes to be in agreement with the experiments of Klebanoff (1971), Kendall (1990), and Westin et al (1994). Lin & Stuckert (1996) have performed similar PSE studies for the response to spanwise vorticity.

The selective mechanisms that convert external disturbances into modes internal to the boundary layer are called *receptivity mechanisms.* The examples in this section show that the PSE method can be used to explore such mechanisms and to incorporate them as part of the analysis.

Nonlinear Problems

At a finite amplitude A, a single mode of frequency ω and spanwise wavenumber β produces harmonics with $\omega_n = n\omega$, $\beta_n = n\beta$, $n = 2, \ldots$, and the steady mean-flow distortion for $n = 0$ owing to the nonlinear term in Equations 4. The amplitudes of the harmonics and mean-flow distortion are of the orders $\mathcal{O}(A^n)$ and $\mathcal{O}(A^2)$, respectively. Similarly, two modes with $n_1\omega$, $m_1\beta$ and $n_2\omega$, $m_2\beta$ produce modes in a pattern of frequencies and wavenumbers governed by the sums and differences $n_1 \pm n_2$, $m_1 \pm m_2$. For simplicity, we denote a mode with $n\omega$ and $m\beta$ by (n, m). The nonlinear evolution of single or multiple modes can be tracked by simultaneously solving a coupled system of PSE for the relevant modes.

The number of relevant modes is usually small near the starting position because $A(x)$ is small, but this number can grow dramatically as the amplitudes increase. Therefore, it is useful to set limits N, M on the highest frequency and wavenumber and hence on the size of the system to be solved.

NONLINEAR GROWTH OF SINGLE MODES An important nonlinear problem, and the first studied by Bertolotti et al (1992), is the development of a single TS

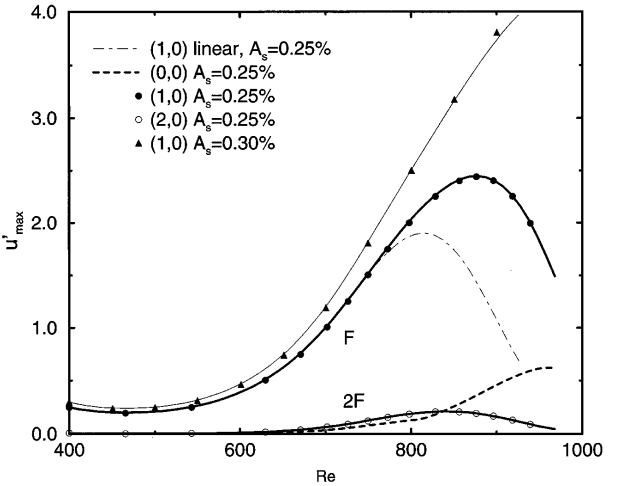

Figure 6 Amplitude $u'_{\max}$ vs *Re* for TS waves at $F = 86 \cdot 10^6$, the mean-flow distortion, and harmonic $2F$ with initial TS amplitude of 0.25% (*heavy lines*) and 0.30% (*thin line*). Results of PSE (*lines*) and DNS (*symbols*). The dash-dot line gives the linear result. (Data of Bertolotti et al 1992.)

wave in the Blasius flow. The PSE results obtained with $N = 5$ and DNS results for a TS wave of frequency $F = 86 \cdot 10^6$ in Figure 6 show good agreement. The main effect of nonlinearity is a destabilization at higher amplitudes that causes a higher maximum amplitude further downstream for $A_s = 0.25\%$ and leads to continuing growth for $A_s = 0.30\%$. These effects have been found in Goldstein & Durbin's (1986) asymptotic analysis. The mean-flow distortion reacts sluggishly to the decay of the TS wave and persists over a long distance downstream. Nonlinear effects on TS waves are weak for amplitudes below 1.5%. This important threshold also applies to wave interactions.

NONLINEAR RECEPTIVITY The receptivity to nonuniform roughness or suction discussed above is a linear mechanism. Crouch (1992) has shown that the interaction of sound with a wavy surface can introduce TS waves. Sound of frequency ω introduces a Stokes layer, whereas a wavy wall of (real) wavenumber α_0 forces a streamwise periodic disturbance. The nonlinear combination of these disturbances resonates strongly near the first neutral point with the TS wave of frequency ω and wavenumber $\alpha \approx \alpha_0$. Crouch & Bertolotti (1992) and Herbert (1994) have successfully repeated this analysis using the PSE approach.

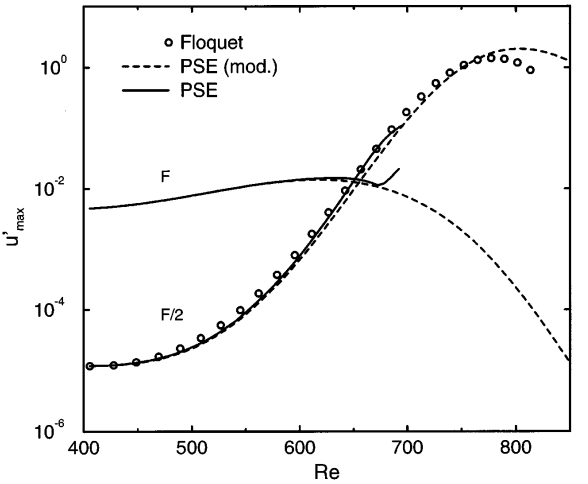

Figure 7 Subharmonic secondary instability of a TS wave with $F = 124 \cdot 10^6$. Comparison between Floquet analysis (*symbols*), modified PSE (*dashed line*), and PSE (*solid line*). (Data of Bertolotti 1991.)

The ability to incorporate such mechanisms into the analysis is important for transition analysis because receptivity provides the link between quantifiable external disturbances and the amplitudes of modes relevant to the transition process.

SECONDARY INSTABILITY Application of Floquet theory of secondary instability (Herbert 1988) requires neglecting nonparallel effects and the amplitude variation of the TS wave. Bertolotti (1991) has solved the PSE to analyze the validity of these assumptions. Results for subharmonic secondary instability are shown in Figure 7. For a direct comparison with the Floquet analysis, the PSE have been modified to suppress the feedback of the 3D subharmonic wave ($F/2$) on the TS wave. The results show only minor deviations. The nonlinear PSE results are in good agreement with Crouch & Herbert's (1993) results.

Similar studies have been performed for other secondary instabilities and show that the PSE capture these important nonlinear mechanisms of the transition process.

TRANSITION SIMULATION It is a small step from the analysis of secondary instability to the simulation of transition by increasing the limits N, M on

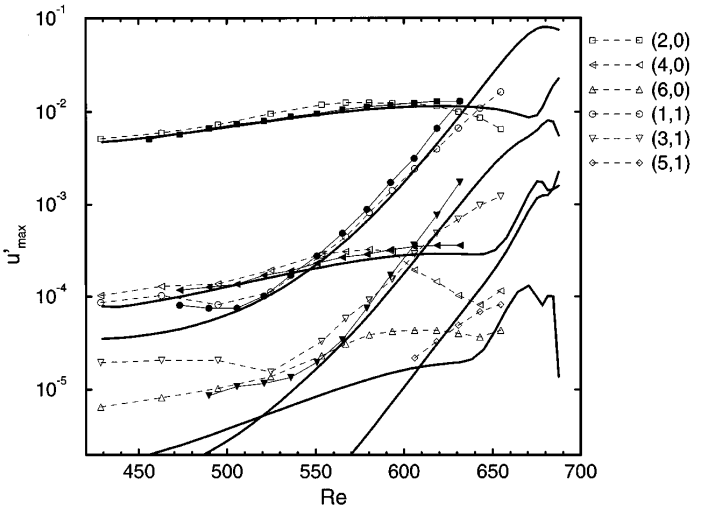

Figure 8 Subharmonic transition for the conditions of Kachanov & Levchenko (1984). Comparison between experiments (*open symbols*), DNS results of Fasel et al (1990) (*closed symbols*), and PSE results with $N = 6$, $M = 3$. (Data of Bertolotti 1991.)

frequency and wavenumber. Bertolotti (1991) performed such simulations for the benchmark experiments of Cornelius (1985) on the K-type of transition (Klebanoff et al 1962) and Kachanov & Levchenko (1984) on the subharmonic route to transition. PSE results with $N = 6$, $M = 3$ for the latter case are compared in Figure 8 with the experiments and DNS results of Fasel et al (1990). The run is started with the TS wave $(2, 0)$ and a subharmonic secondary mode $(1, 1)$ at initial amplitudes that later approach the experimental values. Because of the different transients in experiment, DNS, and PSE, it is difficult to exactly match the amplitudes. The slightly stronger growth of the 3D modes $(1, 1)$ and $(3, 1)$ in the DNS results reflects the slightly higher TS amplitude. The agreement with the experiment is reasonable, except for mode $(4, 0)$. The erratic behavior of the amplitudes near the end of the PSE run is a result of the numerical treatment in this early work. The PSE run continues over an essential region downstream of the end of the DNS run. It is in this region where the skin-friction coefficient C_f reaches a minimum at $Re = 670$ and rises strongly thereafter. This minimum can be used as an operational definition of the transition point.

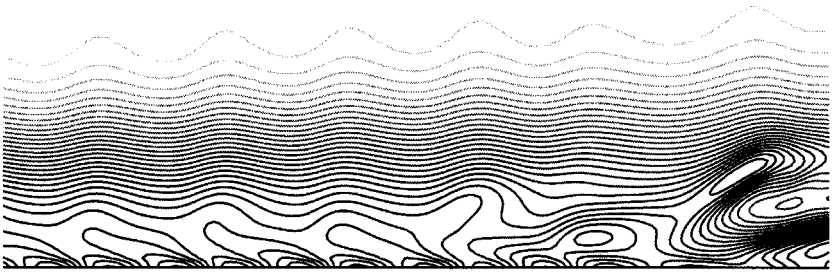

Figure 9 Subharmonic transition for the conditions of Kachanov & Levchenko (1984). Contours of spanwise vorticity in the center plane. The vertical coordinate is scaled 10:1. PSE run with $N = M = 6$.

We have repeated this run with different initial conditions. Starting with LST solutions for the modes $(2, 0)$ and $(1, 1)$, the amplitude evolution of mode $(4, 0)$ shows the same dip near $Re \approx 650$ as the experimental data. Because of the strong effects of minute changes in the initial conditions, the PSE results of different authors for the same case are usually different in some details. Improvements in the solution procedure for the coupled system of PSE permit continuing this run smoothly to the slightly higher Reynolds number $Re = 696$, as shown by the vorticity contours in Figure 9. The earlier CPU times of one hour CRAY-YMP for some nonlinear runs have been cut to a fraction on workstations. Most of the CPU time is used toward the end of the run because the number of modes and the number of iterations per mode increase.

The early results for the nonparallel linear growth of a single mode and the fast transition simulations encouraged Herbert (1991) to propose the PSE approach for more accurate calculations of the growth curves underlying the e^N method and as a nonlinear method for analyzing transition in engineering applications to account for the disturbance environment.

Crossflow and Görtler Instabilities

While the nonparallel effects are small for 2D TS waves and are known for Görtler vortices (Hall 1983), the next step is the analysis of the crossflow vortices in 3D boundary layers. The flow over a rotating disk has been considered in the past (Gregory et al 1955) as a prototype of the flow over a swept wing. Wang (1994) analyzed this flow using the PSE approach and found relatively weak influence of the nonparallel terms. In his analysis of the experiments of Radeztsky et al (1994), he also found that the flow on the rotating disk is not a conclusive example for the flow over swept wings because the

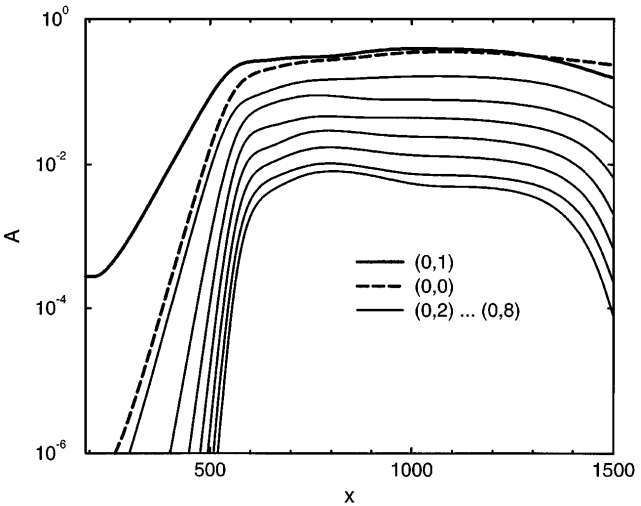

Figure 10 Nonlinear growth of a steady crossflow vortex in swept Hiemenz flow.

boundary-layer thickness is constant. The various families of modes make the analysis of the flow over a rotating disk a challenging yet rather academic problem.

More relevant to the flow over wings is the Hiemenz flow over a swept plate, a special case of the Falkner-Skan-Cooke flow (Cooke 1950) that was the subject of Mack's (1984) detailed stability analysis. Swept Hiemenz flow is unstable to steady and spanwise traveling crossflow modes. In experiments on a similar flow, Müller & Bippes (1988) observed that steady modes dominate at low freestream turbulence. At higher turbulence levels, traveling modes with larger growth rates dominate and exert a stabilizing effect on the simultaneously growing steady modes. Fedorov (1988) found strong excitation of steady vortices by small roughness that was experimentally confirmed by Radeztsky et al (1994, see also Saric 1994a). Crouch (1993) analyzed the relative strength of steady and traveling crossflow vortices, and his results are consistent with Müller & Bippes's experiments.

SINGLE CROSSFLOW MODES The PSE analysis of the linear growth of crossflow vortices in swept Hiemenz flow shows small nonparallel effects. However, the strong growth rapidly leads to large amplitudes and interesting nonlinear effects. The streamwise evolution is shown in Figure 10 for $Re = 500$ and

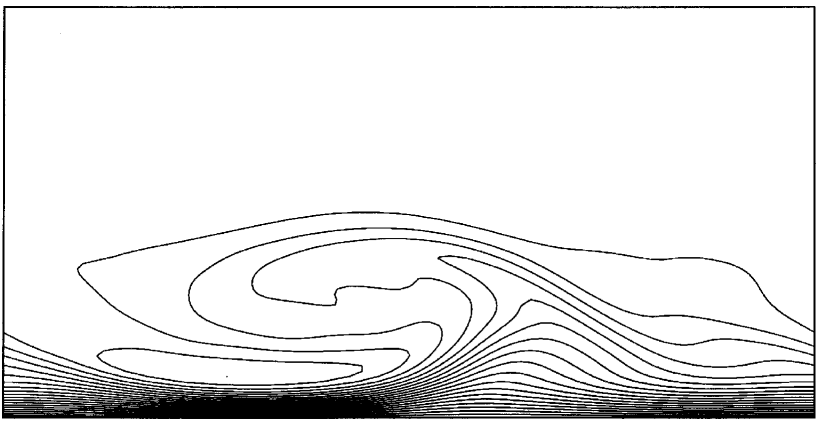

Figure 11 Contour lines of the streamwise velocity at $x = 716$. The contour levels are spaced by 5% of the edge velocity U_e. PSE run with $M = 8$.

$\beta = -0.4$ (Herbert 1994), a case studied with DNS by Spalart (1990) and with PSE by Malik & Li (1992, 1994). Here the Reynolds number Re is formed with the spanwise velocity W_e and the reference length $(\nu/A)^{1/2}$, where $U_e(x) = Ax$. The marching variable x is the Reynolds number formed with U_e. While the linear analysis provides continued growth of $\sigma(x; 0, \beta)$ up to $\sigma > 20$ at $x = 1500$, the nonlinear growth leads to saturation that is largely caused by production of, and interaction with, a strong mean-flow distortion. For $x > 700$, the maximum of the mean-flow distortion $|u_{00}|$ exceeds 10% and the spanwise periodic component $|u_{01}|$ exceeds 17% of the reference velocity W_e. The saturation level depends weakly on the initial amplitude. The skin friction starts to increase significantly before saturation is reached. Similar characteristics have been found for unsteady crossflow vortices.

Figure 11 shows a streamwise cross section of the vortex at $x = 716$ over one period in z and $y \leq 8$ (to scale). The different spacing of the contour lines near the wall indicates a strong spanwise variation of the wall-shear stress. A vertical cut near the center reveals a strongly inflectional velocity distribution. The features we observe in swept Hiemenz flow are consistent with observations of Reibert et al (1996) in the controlled flow over a swept wing.

While the saturation phenomenon in Figure 10 can be obtained with $M = 1$, the detailed structure of the crossflow vortex after saturation depends on the number of harmonics taken into account. The relatively strong influence of harmonics raises questions about the validity of earlier secondary instability results obtained at low truncation.

MODE INTERACTIONS The interaction of steady and traveling modes has been analyzed by Malik & Li (1992, 1994). At a fixed initial amplitude of mode $(0, 1)$, the presence of an unsteady mode $(1, 1)$ reduces the growth of the steady mode and its saturation amplitude. These findings are consistent with the observations of Müller & Bippes. We found the more general result that the mode with the largest amplitude contributes to strengthen the mean-flow distortion. The mean-flow distortion in turn has a damping effect that causes saturation of the largest mode and reduces the growth of other (steady or unsteady) modes present.

Bertolotti (1994) has analyzed a model for the generation of steady crossflow vortices by localized and distributed surface irregularities and tracked the nonlinear development and interaction with traveling modes for Bippes's (Müller & Bippes 1988) flat-plate experiment. The results are consistent with experimental data.

BREAKDOWN OF CROSSFLOW MODES Poll (1985) and Kohama et al (1991) found that the breakdown of crossflow vortices is associated with a high-frequency secondary instability. The frequencies exceed the typical range of TS frequencies in similar flows and the frequencies of unsteady crossflow modes.

The secondary instability of nonlinear steady crossflow vortices has been analyzed by Malik & Li (1993), using the method of 2D eigenfunctions, and by Wang et al (1994), using Floquet analysis. Both studies consider the flow at fixed x as the basic flow and find the secondary instability associated with the embedded shear layers near the edge of the boundary layer. The computational demand of these studies is high because of the numerous modes that constitute the basic flow. PSE studies of the complete breakdown process have not yet been reported.

GÖRTLER VORTICES Saric (1994b) recently reviewed this instability in boundary layers on concave surfaces such as the pressure side of turbine blades. The basic equations for the nonlinear analysis are a special case of the PSE and can be solved without a norm or iteration on α because the streamwise changes can be absorbed into the shape function.

Malik & Li (1993) and Li & Malik (1995) have computed nonlinear Görtler vortices of high amplitude as shown in Figure 12 and analyzed the secondary instability with the method of 2D eigenfunctions. Various modes were found that exhibit different symmetries. By feeding the secondary modes together with the basic flow into a new PSE run, Malik & Li were able to study the further development of the Görtler vortex in the presence of the principal odd and even modes.

Here, as in the case of crossflow vortices, it would be desirable to perform the PSE analysis without the knowledge of the secondary eigenmodes and to

obtain these modes as part of the PSE solution in the more efficient marching procedure. Work toward this objective is in progress.

Compressible Boundary Layers

The extension of the PSE analysis to compressible flows is straightforward. Initial results for boundary layers have been reported for linear modes by Bertolotti & Herbert (1991) and Chang et al (1991), who also presented results for the subharmonic and fundamental breakdown at $Ma = 1.6$. Herbert et al (1993b) used the flat plate for code validation and obtained results on secondary instability in good agreement with those of El-Hady (1991). Chang & Malik (1994) used the PSE for a simulation of the oblique breakdown process at $Ma = 1.6$ without referring to the earlier work of Fasel et al (1991, 1993). Hanifi et al (1995) analyzed the transient growth mechanism in compressible flow.

PRACTICAL APPLICATIONS

For applications other than flat plates, the compressible PSE must be formulated in proper coordinates to accommodate realistic geometries and to reduce the effect of the parabolization. Herbert et al (1993b) and Stuckert et al (1993) have implemented the PSE method in general curvilinear coordinates such that the same code can be adapted to various situations by a relatively simple change

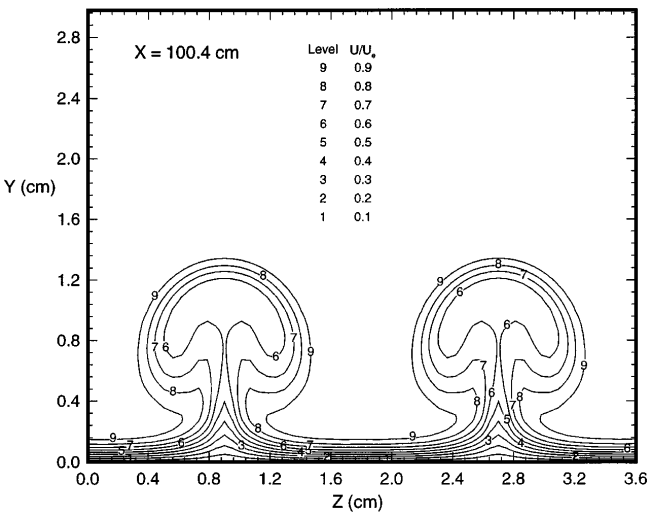

Figure 12 Contour lines of the streamwise velocity at fixed x. The contour levels are spaced by 10% of the edge velocity U_e (Malik & Li 1993).

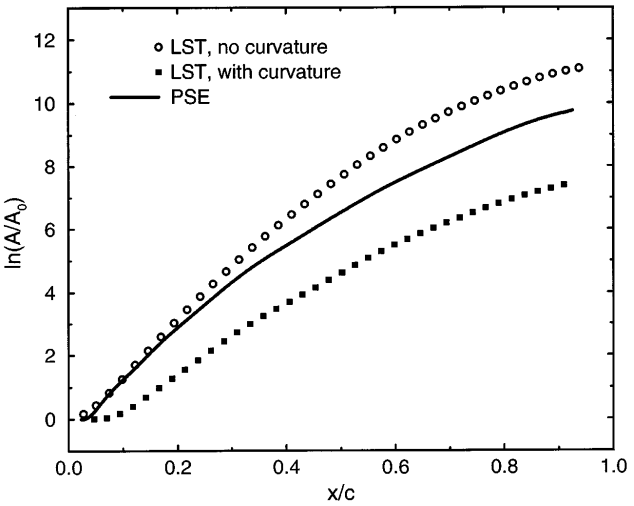

Figure 13 Amplitude growth of a steady crossflow vortex on a swept wing according to the LST with and without curvature in comparison with PSE results.

of the metric. With data for comparison lacking, the code was tested for flat plates, rotating disks, and other cases before analyzing the flows over a blunt cone at $Ma = 8$ and a swept wing at $Ma = 1.5$. To increase the efficiency in applications, a second implementation used the more limited body-intrinsic coordinates for infinite swept wings similar to the codes of Chang et al (1995) and the incompressible code of Haynes & Reed (1996). The implementation by Simen et al (1994) allows for streamwise and spanwise curvature, while the PSE code used by Airiau & Casalis (1994) for an ogive cylinder and the ONERA D airfoil neglects compressibility and metric.

Proper accounting for the metric is important because the growth of disturbances, especially of crossflow vortices on swept wings, is strongly affected by curvature. Accounting for curvature in the LST analysis underestimates the growth to the point where crossflow instability can be suppressed completely. Including curvature in the LST appears to be inconsistent with the parallel-flow assumption in a way similar to including the transverse velocity V alone. Accounting for curvature and the associated changes in the basic flow by using the PSE provides growth weaker than the LST result without curvature but stronger than the LST with curvature, as shown in Figure 13 for a 64A010 swept wing at $Ma = 1.5$ and zero angle of attack.

The main applications for these codes have been incompressible swept wings with the NLF(2)-0415 airfoil (Wang et al 1994, Haynes & Reed 1996), swept wings with the 64A010 airfoil at $Ma = 1.5$ (Stuckert & Herbert 1993, Chang et al 1995), blunt (Herbert et al 1993b) and sharp (Chang & Malik 1993) cones at $Ma = 8$, the swept cylinder of Poll (1985) (Simen et al 1994), a swept cylinder at $Ma = 3.5$ (Chang et al 1995), and the ATTAS flight tests (Schrauf et al 1995, Stolte et al 1995, Herbert & Schrauf 1996). Poll's cylinder has meanwhile evolved into a benchmark for comparison of boundary layers and PSE results because the geometry and pressure distribution are known and nonproprie tary.

Engineering Analysis of Transition

Most PSE applications for realistic geometries so far attempt to reproduce stability characteristics or specific experiments and serve to validate the PSE codes. The problems in practical applications, however, are neither the PSE nor their implementation. The problem is finding the proper input for PSE runs (Herbert 1991, 1996a). The input consists of two major components: the basic flow that determines the coefficients of the PSE, and the external environment that governs initial and boundary conditions. The sensitivity of the transition analysis to small changes requires high quality of the basic flow that cannot always be obtained with the contemporary codes of computational fluid dynamics. The environmental influence is perhaps best illustrated by Figure 14, which was used by Herbert & Morkovin (1980) to discuss the transition issue.

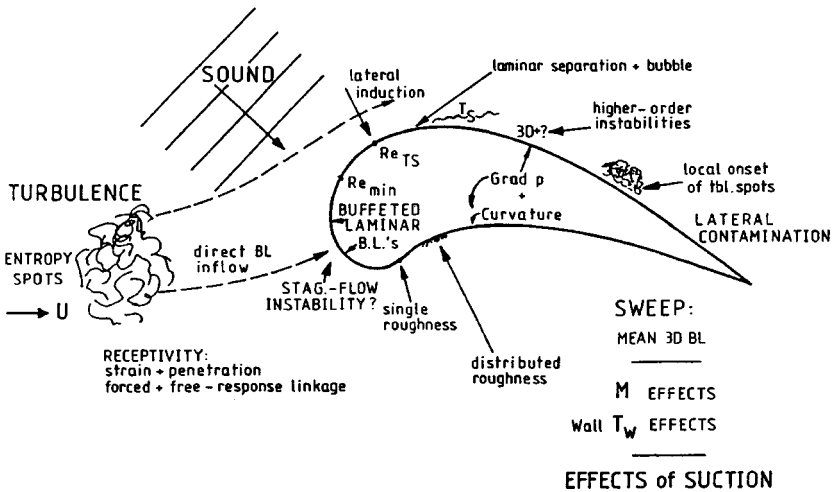

Figure 14 Transition issues in external flows (Herbert & Morkovin 1980).

The scientific approach to capturing the receptivity of boundary layers to the variety of external influences is the development of receptivity models, represented by receptivity coefficients that convert, for example, the turbulence level into an equivalent amplitude of TS waves or unsteady crossflow vortices. The problem in practical applications, however, is even more serious because the external influences are insufficiently known. What is the turbulence level in free flight at different altitudes? What is the sound level in a specific wind-tunnel test?

To overcome the current deficiencies, it is necessary to develop input models with as few as possible tunable parameters that can be empirically adjusted to specific situations. These models are based on the primary and secondary instability characteristics and can be improved as our knowledge of environment, receptivity, and nonlinear mechanisms increases.

Transition on a Turbine Blade

Herbert et al (1993a) studied a group of flows related to transition in the boundary layer of turbine blades at turbulence levels $Tu \geq 0.4\%$. K-type transition is most likely at these turbulence levels. Strong secondary instability of TS waves with respect to low-frequency spanwise modulations requires TS amplitudes in excess of $A^* \approx 1\%$. Up to this limit, nonlinear effects on TS waves are negligible. Given the turbulence level and receptivity coefficient, and assuming equal receptivity in the band of relevant frequencies, the linear amplitude-growth curves can be used to determine the highest frequency TS wave that achieves growth beyond the threshold amplitude A^*. The spanwise modulation is provided by a steady Klebanoff mode or Görtler vortex of a fixed nondimensional wavenumber consistent with observations of Kendall (1991) and in the range of strong secondary instability. The initial amplitude of this vortex is lower than the TS amplitude A_{10} at onset of instability and is less critical. The TS receptivity was estimated to provide an initial amplitude of $A_{10} = 0.3\%$ at $Tu = 0.4\%$, the lowest turbulence level studied by Sohn & Reshotko (1991) in experiments on a heated flat plate. After minor parameter changes, results for the experimental conditions show the rise of the Stanton number St at the observed location and, hence, confirm the validity of this simple model. The location of the minimum of St or C_f is used as an operational definition of the transition location x_{tr}.

For fixed receptivity coefficients, all initial amplitudes increase linearly with the turbulence level. As the TS amplitude increases, the frequency increases and the onset of instability shifts to a lower Reynolds number. Results for the transition location obtained with this simple input model are in good agreement with the experiments at turbulence levels up to $Tu = 2.4\%$. Similar agreement was found with the measurements on convex (Wang et al 1985) and concave

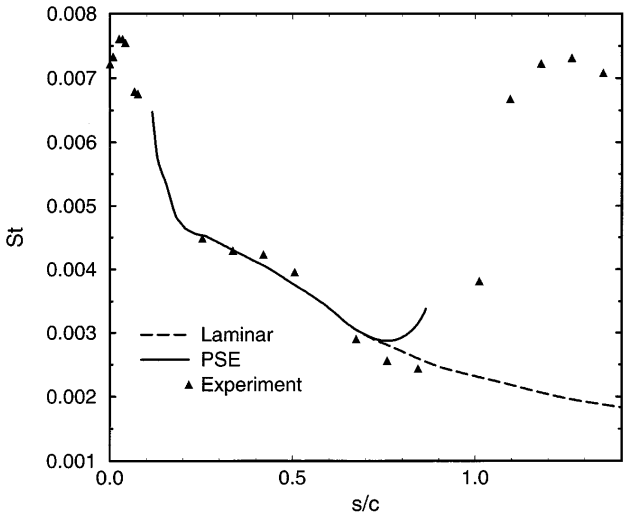

Figure 15 Variation of the Stanton number St with the arclength s/c along a nozzle vane, where c is the chord length (Herbert et al 1993a).

(Kim & Simon 1991) heated plates at $Tu \approx 0.6\%$. Weak convex curvature stabilizes the longitudinal vortex and shifts x_{tr} slightly downstream. Kim & Simon attributed the early rise of St on concave walls to bypass transition. The PSE results show instead that the concave curvature causes a strong Görtler vortex that affects the heat transfer without participation of the TS wave and before breakdown.

For the nozzle vane of the annular stator in the experiments by Dring et al (1986), the basic flow at mid-span was obtained using a 2D panel code and a boundary-layer code. After a survey of the linear stability of the flow, the input model was adapted to the turbulence level $Tu = 0.5\%$. The PSE results for the variation of the Stanton number along the arclength s/c on the suction side are shown in Figure 15, together with the laminar values and experimenta data.

The PSE run provides a transition location somewhat upstream of the experimental value. Although some of this difference may be attributed to the simple input model, we see the main reason in the deviation between computed and actual laminar flow in the experiments. Comparison with a Navier-Stokes solution for the basic flow reveals that this deviation is caused by three-dimensionality and the use of the lowest boundary-layer approximation in the narrow passage.

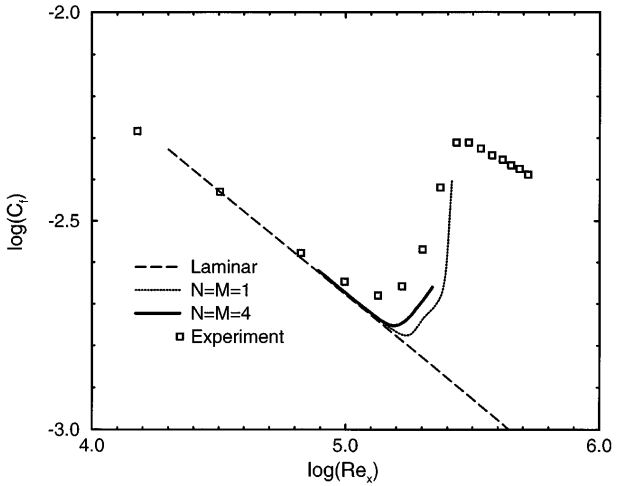

Figure 16 Transition for test case T3A at $Tu = 3\%$. Comparison of PSE result and experimental data (Savill 1992).

We have recently applied the same input model to the ERCOFTAC test case T3A (Savill 1992) at $Tu = 3\%$ and obtained the results shown in Figure 16. The agreement with the experimental data is comparable with DNS results for this test case. The lower minimum and steeper rise of C_f in the PSE result may be attributed to the neglect of intermittency. Our result indicates that instability mechanisms are still at work in this case of "bypass transition." The turbulence level of 3% is near the upper limit for PSE applications, as long as we have no better grasp on the receptivity to high free-stream turbulence.

Airiau & Casalis used a similar input model in the PSE analysis of the flows over an ogive cylinder and the ONERA D airfoil. For the turbulence level $Tu = 0.15\%$ of wind-tunnel tests, they find the onset of strong K-type resonance in a close range of $\ln(A/A_0) \approx 5.5$.

TS-Wave–Dominated Transition in Flight Tests

The disturbance environment in free flight is largely unknown. Developing an input model for this situation requires access to mostly proprietary flight-test data. Schrauf (1994) has evaluated different e^N strategies for the ATTAS flight tests that were carried out on the laminar-flow glove of a VFW 614 aircraft in the range of $0.35 \leq Ma \leq 0.7$ and $12 \cdot 10^6 \leq Re \leq 30 \cdot 10^6$. The sweep angle was varied from 18 to 24 degrees by flying with sideslip such that the

test envelope covered the range from dominating TS instability to dominating crossflow instability.

Schrauf et al (1995) have performed a PSE analysis of selected TS-dominated cases to study transition mechanisms on swept wings and to develop input models. The secondary instability mechanisms for 2D flows (Herbert 1988) were tracked for increasing sweep angles and were found to carry over to 3D flows with minor changes. Owing to the loss of symmetry across the edge streamline, the "left" and "right" subharmonic waves (1, 1) and (1, −1) initially show different characteristics, but they synchronize and grow simultaneously as the growing TS wave strengthens the parametric instability. Assuming uniform receptivity for waves, the initial amplitudes of the subharmonic waves were chosen such that their amplitudes would not decrease below the initial amplitude of the TS wave. K-type resonance occurs primarily in combination with weakly amplified crossflow vortices.

Starting from a diagram of linear amplitude-growth curves, the "most dangerous" parameter combinations were identified by numerous PSE runs. PSE runs with fixed initial amplitude of the crossflow mode provide the variation of the transition location with the initial TS amplitude, as shown in Figure 17 for subharmonic transition in ATTAS case B.

In-flight infrared photographs for case B exhibit transition near 40% chord. According to Figure 17, the transition location can be attributed to an amplitude level of waves in the range of $2 - 3 \cdot 10^{-6}$. Similar levels of $1 - 3 \cdot 10^{-6}$ lead to K-type or subharmonic transition in another test case A, where transition is observed at 17% chord. The amplitude of the crossflow vortex in the K-type model has been varied over two orders of magnitude but causes only a small shift of less than 1% chord.

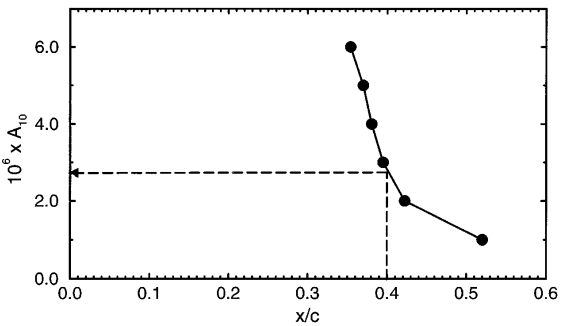

Figure 17 Variation of the transition location with the disturbance level A_{10} for subharmonic resonance in ATTAS test case B.

Determining whether these disturbance levels vary with altitude and other flight conditions requires evaluating the results of other flight tests. The broader validity of the estimated disturbance levels is supported by the e^N method. With $N = 9$ and $A_0 = 2 \cdot 10^{-6}$, this method predicts transition when the TS wave reaches an amplitude of 1.6%, shortly downstream of the onset of strong secondary instability.

The analysis by Schrauf et al (1995) suggests that the e^N method can provide information on TS-dominated transition in 2D and 3D boundary layers, provided that N is determined properly. This conclusion agrees with Arnal's findings (1994, see also Reed et al 1996).

Crossflow-Dominated Transition in Flight Tests

PSE studies of nonlinear crossflow instability in swept Hiemenz flow have concentrated on the evolution of single modes or the interaction between single steady and unsteady modes. Flows over swept wings are different, though, since the significant growth of the boundary layer causes the range of unstable steady and unsteady crossflow modes to change from high wavenumbers near the leading edge to much lower wavenumbers downstream. Herbert & Schrauf (1996) have analyzed the nonlinear phenomena for the crossflow-dominated ATTAS flight test case C starting from the chart of linear amplitude-growth curves in Figure 18.

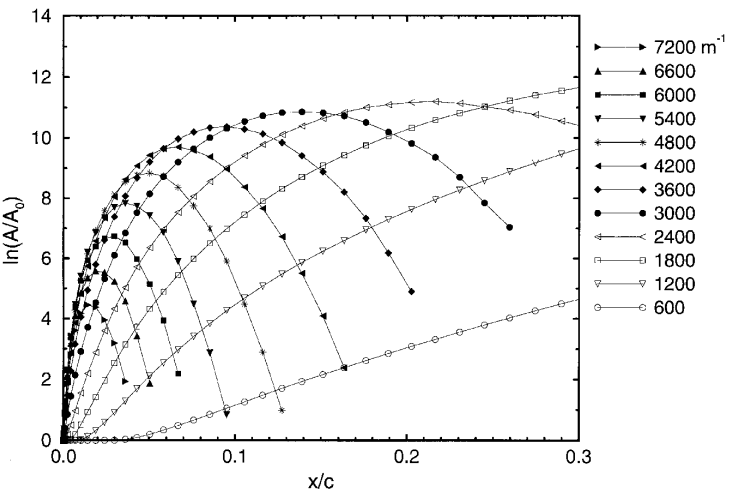

Figure 18 Growth curves for steady crossflow vortices of different wavenumbers along x/c, where c is the chord length.

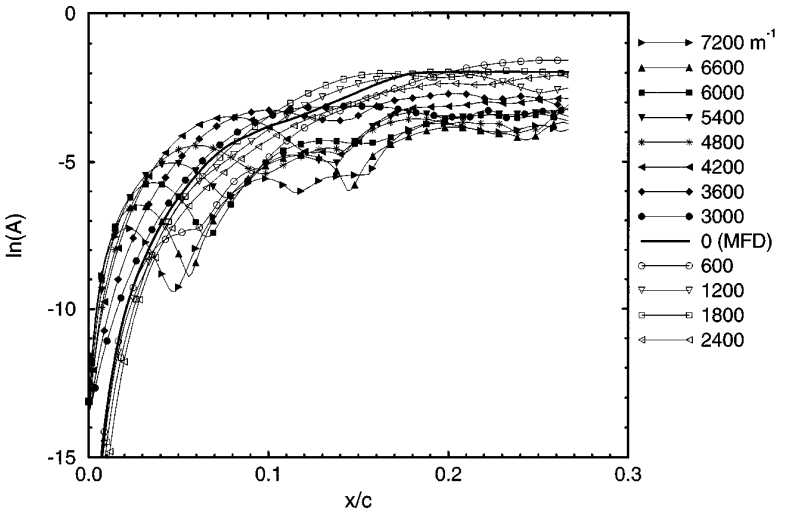

Figure 19 Interaction of steady crossflow vortices of different wavenumbers with $A_{0m} = 2 \cdot 10^{-6}$ for modes with $\beta \geq 3000\ \mathrm{m}^{-1}$.

As in swept Hiemenz flow, single, continuously amplified crossflow modes of low wavenumbers can grow nonlinearly to large, slowly varying saturation amplitudes that depend weakly on the initial amplitudes. Single modes of high wavenumbers grow nonlinearly to a maximum amplitude and then decay, leaving behind a mean-flow distortion (MFD) that decays on its own viscous scale. This behavior has also been found by Stolte et al (1995). In interactions between steady and traveling modes, the largest mode reduces the growth of smaller modes through the MFD that also causes the largest mode to saturate if it is linearly unstable.

The infrared record for case C exhibits the characteristic zigzag pattern of crossflow-dominated transition between 15% and 28% chord. The steady pattern suggests that transition originates from distributed roughness and steady crossflow modes. Crouch (1994) found that the nonlocalized receptivity to roughness produces a broad band of steady modes, especially in the leading-edge region. Herbert & Schrauf have performed PSE runs that track the nonlinear evolution of discrete modes in the broad band of unstable wavenumbers. Figure 19 gives the result for a run that started with uniform initial amplitudes of $A_{0m} = 2 \cdot 10^{-6}$ for the eight modes with wavenumbers between 3000 m^{-1} to 7200 m^{-1} that are marked by the full symbols in Figures 18 and 19.

Some discrepancies between the linear and nonlinear cases are immediately clear: None of the modes decay in Figure 19, and for $x/c > 0.1$ the flow is dominated by low-wavenumber modes (open symbols) that were not introduced by the initial conditions and are expected from Figure 18 to exhibit modest growth. The mode with the smallest wavenumber of 600 m^{-1} is the lowest in Figure 18 but is highest at the end of the nonlinear run. The highest amplitudes at $x/c = 0.3$ exceed 25%. The underlying mechanisms are known. Initially, the high-wavenumber modes grow and create the mean-flow distortion and new modes at their wavenumber difference. Farther downstream, the strengthened low-wavenumber modes maintain the modes with higher wavenumbers as harmonics and at the sum of their wavenumbers. In special runs, Herbert & Schrauf found that this process continues to modes of very low wavenumbers qualitatively and quantitatively similar to the MFD. The zigzag pattern of crossflow-dominated transition is a result of the simultaneous growth of modes in a broad band of wavenumbers.

Figure 19 brings good news and bad news for the aerodynamic designer. The bad news is that use of the linear data in Figure 18 can lead the design in the wrong direction. This conclusion is also valid for cases with weaker crossflow instability where $\ln(A/A_0)$ remains below values of $N = 6$. The good news is that we know why the e^N method tends to fail for crossflow vortices. This failure is caused by the combination of the saturation process with the nonlinear interaction of a broad band of modes.

Work is in progress to utilize the results of a single run to construct a model of these processes and to convert the linear data to an approximation of the nonlinear data for similar situations, so that the design engineer does not need to wait for the result of tedious nonlinear computations. The still unsolved problem of simulating the breakdown of crossflow vortices will probably be solved by the time this review appears.

Advanced Applications

The research and commercial potential of the PSE has created competing groups with relatively sparse communication on improvements in this field. Therefore, it is difficult to provide a complete overview of research directions.

3D BOUNDARY LAYERS Our current efforts and those by Arnal (personal communication) are directed at solving the PSE for fully 3D boundary layers as they appear, for example, on a wing in the neighborhood of the engines. In this case, Equation 13 must be solved in an extended marching procedure subject to two norms (Equations 9a and 9b) under constraint by the irrotationality condition

(Equation 12b) and with complex-valued β. Herbert (1996b) presented results of this procedure for an infinite swept wing (Poll's cylinder at 63 degrees sweep) with heated panels. These panels are representative of the wing areas over the fuel tank when an aircraft has climbed from ground level to cruising altitude. The variation of the N factor in the 3D boundary layer deviates significantly from the LST results and from those of the PSE for quasi-3D flows (Equations 14 and 9a). A major part of the differences arises from the propagation of the disturbances along a path related to, but different from, the edge streamlines. Current work aims at clarification of the growth characteristics, comparison with previously applied concepts, and improving the accuracy of the basic flow by using a 3D boundary-layer code. In the absence of microscopic experiments and theoretical results, solving the complete 3D PSE closes an important gap in our ability to analyze aerodynamic flows.

ADJOINT LINEAR PSE Guided by the successful use of adjoint methods to restabilize wakes (Hill 1992), Hill (1995) showed that the solution of the adjoint LST problem is closely related to linear receptivity problems. The adjoint solution defines the sensitivity of a chosen disturbance to modifications of the basic flow or boundary conditions. To account for streamwise variations and surface curvature effects, the adjoint linear compressible PSE can be utilized to analyze the sensitivity of disturbances in aerodynamic boundary layers. In contrast to the regular PSE, the adjoint PSE calculation is marched in the upstream direction.

While contour plots of the adjoint components directly reveal the response of the disturbance to changes (e.g. of the normal velocity at the wall), the inhomogeneous combination with the downstream solution can be used to provide a direct measure of the receptivity (e.g. to a suction strip at a certain location). Adjoint and regular PSE solutions can be exploited in an inverse design method to determine the most effective laminar flow control strategy for any type of instability mode. The method can provide the optimum placement of suction panels or the modifications to the airfoil that most efficiently reduce the growth of an unstable mode.

As an example of an adjoint PSE solution, Figure 20 shows the adjoint pressure for traveling crossflow vortices on Poll's (1985) swept cylinder. The largest values of the adjoint pressure field occur close to the neutral point for the disturbance. Excitation by a normal velocity at the wall that is introduced at the location where the adjoint field has maximum wall values will induce the largest traveling vortex. The determination of a control strategy for the traveling vortex requires the solution of a second, inhomogeneous adjoint PSE problem.

Figure 20 The adjoint pressure for traveling crossflow vortices on Poll's cylinder at 63 degree sweep for $f = 1\text{kHz}$, $\beta = 1600\ \text{m}^{-1}$, $Re = 1.47 \cdot 10^6$. The distance from the wall is scaled 20:1.

CLOSURE

In less than a decade since their conception, the parabolized stability equations have developed into a mature approach to analyze the receptivity, linear, and nonlinear stability of convectively unstable flows into the late stages of transition. Applications cover the range from incompressible to hypersonic flows and increasingly contribute to the fundamentals of fluid mechanics.

Applications of the PSE approach for transition analysis in realistic aerodynamic flows have made encouraging progress toward accounting for the disturbance environment and locating the transition point on the basis of nonlinear changes in skin-friction or heat transfer. The small number of empirical parameters in the input model for PSE runs will soon be replaced by better documentation of the disturbance environment and quantitative analysis of the receptivity coefficients.

The ease of studying nonlinear processes on a workstation is a great reward for the considerable effort expended in developing an advanced PSE code. In 1966, my teacher Walter Tollmien entrusted to me his dream of combining the computer, stability theory, and methods of applied mathematics to create

Turbulenz aus der Retorte (synthetic turbulence). A good part of this dream has come true.

ACKNOWLEDGMENTS

I dedicate this paper to Dr. Leslie M. Mack for his contributions to the linear stability of three-dimensional and compressible flows. I have benefited not only from his work and many fruitful discussions but equally from knowing him as an honest colleague and friend.

I am indebted to Dr. Seppo Korpela, Dr. Chris Hill, and Charlotte Herbert for their valuable comments on the original manuscript. The development and evaluation of the PSE method have been supported by the Air Force Office of Scientific Research. The codes for compressible PSE analysis in general curvilinear coordinates have been developed in cooperation with Drs. G. K. Stuckert, N. Lin, S. Huang, and D. C. Hill. This work has been supported by Wright Laboratories, NASA Ames Research Center, and NASA Lewis Research Center. The ongoing analysis of the ATTAS flight tests is conducted in cooperation with Dr. G. Schrauf, Daimler-Benz Aerospace Airbus GmbH, and is supported by the German technology program RaWiD. I am grateful for the generous sharing of information in this effort.

Literature Cited

Airiau C. 1994. *Stabilité linéaire et faiblement non linéaire d'une couche limite laminaire incompressible par un système d'equations parabolisé (PSE)*. PhD thesis, L'École Nationale Supérieure de L'Aeronautique et de L'Espace, Toulouse

Airiau C, Casalis G. 1994. Nonlinear PSE compared with DNS and experiment. In *Laminar-Turbulent Transition*, ed. R. Kobayashi, pp. 85–92. New York: Springer Verlag

Arnal D. 1984. Description and prediction of transition in two-dimensional, incompressible flow. In *Special Course on Stability and Transition of Laminar Flow*, pp. 2/1–71. *AGARD Rep. No. 709*

Arnal D. 1994. Boundary layer transition: predictions based on linear theory. In *Special Course on Progress in Transition Modelling*, pp. 2/1–63. *AGARD Rep. No. 793*

Balakumar P, Malik MR. 1992. Waves produced from a harmonic point source in a supersonic boundary-layer flow. *J. Fluid Mech.* 245:229–47

Bertolotti FP. 1989. Nonlinear analysis of boundary layers with streamwise varying properties. *Annu. Rep., NASA Training Grant NGT 50259*

Bertolotti FP. 1991. *Linear and nonlinear stability of boundary layers with streamwise varying properties*. PhD thesis, Ohio State Univ., Columbus

Bertolotti FP. 1994. A partial simulation of recepitivity and transition in 3-D boundary layers. In *Laminar-Turbulent Transition*, ed. R Kobayashi, pp. 491–98. New York: Springer Verlag

Bertolotti FP. 1996. Response of the Blasius boundary layer to free-stream vorticity. *Phys. Fluids*. Submitted

Bertolotti FP, Herbert Th. 1991. Analysis of the linear stability of compressible boundary layers using the PSE. *Theor. Comp. Fluid Dyn.* 3:117–24

Bertolotti FP, Herbert Th, Spalart PR. 1992. Linear and nonlinear stability of the Blasius boundary layer. *J. Fluid Mech.* 242:441–74

Bouthier M. 1972. Stabilité linéairé des écoulements presque parallèles. *J. Mécanique* 11:599–621

Bouthier M. 1973. Stabilité linéairé des écoulements presque parallèles. Part II. La couche limite de Blasius. *J. Mécanique* 12:75–95

Butler KM, Farrell BF. 1992. Optimal perturbations and streak spacing in wall-bounded

turbulent shear flow. *Phys. Fluids A* 5:774–77
Chang C-L, Malik MR. 1993. Non-parallel stability of compressible boundary layers. *AIAA Pap. No. 93-2912*
Chang C-L, Malik MR. 1994. Oblique-mode breakdown and secondary instability in supersonic boundary layers. *J. Fluid Mech.* 273:323–60
Chang C-L, Malik MR, Erlebacher G, Hussaini MY. 1991. Compressible stability of growing boundary layers using parabolized stability equations. *AIAA Pap. No. 91-1636*
Chang C-L, Malik MR, Vinh H. 1995. Linear and nonlinear stability of compressible swept-wing boundary layers. *AIAA Pap. No. 95-2278*
Cooke JC. 1950. The boundary layer of a class of infinite yawed cylinders. *Proc. Cambridge Phil. Soc.* 46:645–48
Cornelius KC. 1985. Three dimensional wave development during boundary layer transition. *Lockheed Georgia Res. Rep. No. LG85RR0004*
Crouch JD. 1992. Non-localized receptivity of boundary layers. *J. Fluid Mech.* 224:567–81
Crouch JD. 1993. Receptivity of three-dimensional boundary layers. *AIAA Pap. No. 93-0074*
Crouch JD. 1994. Theoretical studies on the receptivity of boundary layers. *AIAA Pap. No. 94-2224*
Crouch JD, Bertolotti FP. 1992. Nonlocalized receptivity of boundary layers to three-dimensional disturbances. *AIAA Pap. No. 92-0740*
Crouch JD, Herbert Th. 1993. Nonlinear evolution of secondary instabilities in boundary-layer transition. *Theor. Comp. Fluid Dyn.* 4:151–75
Dring RP, Blair MF, Joslyn HD, Power GD, Verdon JM. 1986. The effects of inlet turbulence and rotor/stator interactions on the aerodynamics and heat transfer of a large-scale rotating turbine model. *NASA CR 4079*
El-Hady NM. 1991. Spatial three-dimensional secondary instability of compressible boundary-layer flows. *AIAA J.* 29:688–96
Fasel H, Thumm A, Bestek H. 1993. Direct numerical simulation of transition in supersonic boundary layers: oblique breakdown. In *Transitional and Turbulent Compressible Flows*. ASME-FED
Fasel HF, Rist U, Konzelman U. 1990. Numerical investigation of the three-dimensional development in boundary-layer transition. *AIAA J.* 28:29–37
Fasel HF, Thumm A. 1991. Numerical simulation of three-dimensional breakdown in supersonic boundary layer transition. *Bull. Am. Phys. Soc.* 36:2701
Fedorov AV. 1988. Excitation of waves of instability of the secondary flow in the boundary layer on a swept wing. *Z. PMTF* 5:46–52
Gaster M. 1962. A note on the relation between temporally-increasing and spatially-increasing disturbances in hydrodynamic stability. *J. Fluid Mech.* 14:222–24
Gaster M. 1974. On the effects of boundary-layer growth on flow stability. *J. Fluid Mech.* 66:465–80
Gaster M. 1975. A theoretical model of a wave packet in the boundary layer on a flat plate. *Proc. R. Soc. London Ser. A.* 347:271–89
Goldstein ME, Durbin PA. 1986. Nonlinear critical layers eliminate the upper branch of spatially growing Tollmien-Schlichting waves. *Phys. Fluids* 29:2344–55
Görtler H. 1940. Über eine dreidimensionale Instabilität laminarer Grenzschichten an konkaven Wänden. *Nachr. Ges. Wiss. Göttingen, N.F.* 2:1–26
Gray WE. 1952. The effect of wing sweep on laminar flow. *R.A.E. Tech. Memo. 255*
Gregory N, Stuart JT, Walker WS. 1955. On the stability of three-dimensional boundary layers with application to the flow due to a rotating disk. *Philos. Trans. R. Soc. London Ser. A* 248:155–99
Haj-Hariri H. 1994. Characteristics analysis of the parabolized stability equations. *Stud. Appl. Math.* 92:41–53
Hall P. 1983. The linear development of Görtler vortices in growing boundary layers. *J. Fluid Mech.* 130:41–58
Hanifi A, Schmid PJ, Henningson DS. 1996. Transient growth in compressible boundary layers. *Phys. Fluids*. Submitted
Haynes TS, Reed HL. 1996. Computations in nonlinear saturation of stationary crossflow vortices in a swept-wing boundary layer. *AIAA Pap. No. 96-0182*
Herbert Th. 1988. Secondary instability of boundary layers. *Annu. Rev. Fluid Mech.* 20:487–526
Herbert Th. 1991. Boundary-layer transition – analysis and prediction revisited. *AIAA Pap. No. 91-0737*
Herbert Th. 1994. Parabolized stability equations. In *Special Course on Progress in Transition Modelling*, pp. 4/1–34. *AGARD Rep. No. 793*
Herbert Th. 1996a. On the status of applied transition analysis. In *Transitional Boundary Layers in Aeronautics*, ed. RAWM Henkes, JL Van Ingen. Amsterdam: Elsevier. In press
Herbert Th. 1996b. Progress in applied transition analysis. *AIAA Pap. No. 96-1993*
Herbert Th, Bertolotti FP. 1987. Stability analysis of nonparallel boundary layers. *Bull. Am. Phys. Soc.* 32:2079

Herbert Th, Lin N. 1993. Studies on boundary-layer receptivity with parabolized stability equations. *AIAA Pap. 93-3053*

Herbert Th, Morkovin MV. 1980. Dialogue on bridging some gaps in stability and transition research. In *Laminar-Turbulent Transition*, ed. R Eppler, H Fasel, pp. 47–72. New York: Springer-Verlag

Herbert Th, Schrauf G. 1996. Crossflow-dominated transition in flight tests. *AIAA Pap. No. 96-0185*. Submitted to *AIAA J.*

Herbert Th, Stuckert GK, Esfahanian V. 1993a. Effects of free-stream turbulence on boundary-layer transition. *AIAA Pap. No. 93-0488*

Herbert Th, Stuckert GK, Lin N. 1993b. Method for transition prediction in high-speed boundary layers. *Wright Lab., Rep. No. WL-TR-93-3097*

Hill DC. 1992. A theoretical approach for analyzing the stabilization of wakes. *AIAA Pap. No. 92-0007*

Hill DC. 1995. Adjoint systems and their role in the receptivity problem for boundary layers. *J. Fluid Mech.* 292:183–204

Huerre P, Monkewitz PA. 1990. Local and global instabilities in spatially developing flows. *Annu. Rev. Fluid Mech.* 22:473–537

Kachanov YS. 1994. Experiments on boundary-layer transition. *Annu. Rev. Fluid Mech.* 26:411–82

Kachanov YS, Kozlov VV, Levchenko VY. 1975. Growth of small disturbances in a boundary layer. *Ucheniye Zapiski TSAGI* 6:137–40

Kachanov YS, Levchenko VY. 1984. The resonant interaction of disturbances at laminar-turbulent transition in a boundary layer. *J. Fluid Mech.* 138:209–47

Kendall JM. 1990. Boundary layer receptivity to freestream turbulence. *AIAA Pap. No. 90-1504*

Kendall JM. 1991. Studies on laminar boundary layer receptivity to freestream turbulence near a leading edge. In *Boundary Layer Stability and Transition to Turbulence*, ed. DC Reda, HL Reed, R Kobayashi, 114:23–30. ASME FED

Kim J, Simon TW. 1991. Free-stream turbulence and concave curvature effects on heated, transitional boundary layers. *Tech. Rep., NASA CR 187150*

Klebanoff PS. 1971. Effect of free-stream turbulence on a laminar boundary layer. *Bull. Am. Phys. Soc.* 16:1323

Klebanoff PS, Tidstrom KD, Sargent LM. 1962. The three-dimensional nature of boundary-layer instability. *J. Fluid Mech.* 12:1–34

Kohama Y, Saric WS, Hoos JA. 1991. A high-frequency secondary instability of crossflow vortices that leads to transition. In *Boundary Layer Transition and Control, Cambridge, UK*, pp. 4.1–4.13. Cambridge: R. Aeronaut. Soc.

Li F, Malik MR. 1994. Mathematical nature of parabolized stability equations. In *Laminar-Turbulent Transition*, ed. R Kobayashi, pp. 205–12. New York: Springer Verlag

Li F, Malik MR. 1995. Fundamental and subharmonic secondary instabilities of Görtler vortices. *J. Fluid Mech.* 297:77–100

Liepmann HW. 1943. Investigation of laminar boundary layer stability and transition on curved boundaries. *NACA Adv. Conf. Rep. No. W-107*

Lin N, Stuckert GK. 1996. Boundary layer receptivity to freestream vortical disturbances. *Phys. Fluids*. Submitted

Mack LM. 1969. Boundary-layer stability theory. Jet Propulsion Lab., Pasadena, CA, *Doc. No. 900-277, Rev. A*

Mack LM. 1977. Transition prediction and linear stability theory. In *Laminar-Turbulent Transition*, pp. 1/1–22. *AGARD CP 224*

Mack LM. 1984. Boundary-layer linear stability theory. In *Special Course on Stability and Transition of Laminar Flow*, pp. 3/1–81. *AGARD Rep. No. 709*

Mack LM, Herbert Th. 1995. Linear wave motion from concentrated harmonic sources in Blasius flow. *AIAA Pap. No. 95-0774*

Mack LM, Kendall JM. 1983. Wave pattern produced by a localized harmonic point source in a Blasius boundary layer. *AIAA Pap. No. 83-0046*

Malik MR, Li F. 1992. Three-dimensional boundary layer stability and transition. *SAE Pap. No. 921991*

Malik MR, Li F. 1993. Secondary instability of Görtler and crossflow vortices. In *Proc. Int. Symp. Aerospace Fluid Sci.*, pp. 460–77. Sendai, Japan: Tohoku Univ.

Malik MR, Li F. 1994. Crossflow disturbances in three-dimensional boundary layers: nonlinear development, wave interaction and secondary instability. *J. Fluid Mech.* 268:1–36

Müller B, Bippes H. 1988. Experimental study of instability modes in a three-dimensional boundary layer. In *Fluid Dynamics of Three-Dimensional Turbulent Shear Flows. AGARD CP 438*

Orr WM. 1907. The stability or instability of the steady motions of a perfect liquid and a viscous liquid. *Proc. R. Irish Acad. A* 27:9–27, 69–138

Poll DIA. 1985. Some observations of the transition process on the windward face of a long yawed cylinder. *J. Fluid Mech.* 150:329–56

Prandtl L. 1921. Bemerkungen über die Entstehung der Turbulenz. *ZAMM* 1:481–63

Prandtl L. 1922. Bemerkungen über die Entstehung der Turbulenz. *Phys. Z.* 23:19–23

Radeztsky RH, Reibert MS, Saric WS. 1994. Development of stationary crossflow vortices on a swept wing. *AIAA Pap. No. 94-2373*

Reddy SC, Henningson DS. 1993. Energy growth in viscous channel flows. *J. Fluid Mech.* 252:209–38

Reed HL, Saric WS, Arnal D. 1996. Linear stability theory applied to boundary layers. *Annu. Rev. Fluid Mech.* 28:389–428

Reibert MS, Saric WS, Carillo RB Jr, Chapman KL. 1996. Experiments in nonlinear saturation of stationary crossflow-vortices in a swept-wing boundary layer. *AIAA Pap. No. 96-0184*

Reynolds O. 1883. An experimental investigation of the circumstances which determine whether the motion of water shall be direct or sinuous, and of the law of resistance in parallel channels. *Philos. Trans. R. Soc. London* 174:935–82

Saric WS. 1989. Low-speed experiments: requirements for stability measurements. In *Instability and Transition*, ed. MY Hussaini, RG Voigt, 1:162–74. New York: Springer Verlag

Saric WS. 1994a. Physical description of boundary-layer transition: experimental evidence. In *Special Course on Progress in Transition Modelling*, pp. 3/1–51. *AGARD Rep. No. 793*

Saric WS. 1994b. Görtler vortices. *Annu. Rev. Fluid Mech* 26: 379–409

Saric WS, Nayfeh AH. 1977. Nonparallel stability of boundary layers with pressure gradients and suction. In *Laminar-Turbulent Transition*, pp. 6/1–21. *AGARD CP 224*

Savill AM. 1992. A synthesis of T3 test case predictions. In *Numerical Simulation of Unsteady Flows and Transition to Turbulence*, ed. O Pironneau, W Rodi, IL Ryhmig, AM Savill, TV Truong, pp. 404–42. Cambridge: Cambridge Univ. Press

Schlichting H. 1933. Zur Entstehung der Turbulenz bei der Plattenströmung. *Nachr. Ges. Wiss. Göttingen, Math.-Phys. Kl.*, pp. 181–208

Schmid PJ, Henningson DS. 1992. A new mechanism for rapid transition involving a pair of oblique waves. *Phys. Fluids A* 4:1986–89

Schrauf G. 1994. Transition prediction using different linear stability analysis strategies. *AIAA Pap. No. 94-1848*. Submitted to *AIAA J. Aircraft*

Schrauf G, Herbert Th, Stuckert GK. 1995. Evaluation of transition in flight tests using nonlinear PSE analysis. *AIAA J. Aircraft* 33:554–60

Schubauer GB, Skramstad HK. 1943. Laminar boundary-layer oscillations and transition on a flat plate. *NACA Adv. Conf. Rep. No. W-8*

Schubauer GB, Skramstad HK. 1947. Laminar boundary-layer oscillations and transition on a flat plate. *J. Res. Nat. Bur. Stand* 38:251–92

Simen M. 1992. Local and nonlocal stability theory of spatially varying flows. In *Instability, Transition and Turbulence*, pp. 181–201. New York: Springer Verlag

Simen M, Bertolotti FP, Hein S, Hanifi A, Henningson D, Dallmann U. 1994. Nonlocal and nonlinear instability theory. In *Proc. ECCOMAS Conf. on Computational Fluid Dynamics*, ed. S Wagner, J Périaux, EH Hirschel. Wiley

Simen M, Hein S, Bertolotti F, Wendt V, Hanifi A, Henningson D. 1994. Nonlocal and local instability analysis of hypersonic flows. In *Laminar-Turbulent Transition*, ed. R Kobayashi, pp. 147–54. New York: Springer Verlag

Smith AMO, Gamberoni AH. 1956. Transition, pressure gradient and stability theory. *Douglas Aircraft Co. Rep. No. ES26388*

Sohn KH, Reshotko E. 1991. Experimental study of boundary layer transition with elevated freestream turbulence on a heated flat plate. *NASA TM 187068*

Sommerfeld A. 1908. Ein Beitrag zur hydrodynamischen Erklärung der turbulenten Flüssigkeitsbewegung. In *Atti del 4. Congr. Internat. dei Mat., III*, pp. 116–24. Roma

Spalart PR. 1990. Direct numerical study of cross-flow instability. In *Laminar-Turbulent Transition*, ed. R Michel, D Arnal, pp. 621–30. New York: Springer Verlag

Squire HB. 1933. On the stability for three-dimensional disturbances of viscous fluid flow between parallel walls. *Proc. R. Soc. London Ser. A.* 142:621–28

Stolte A, Bertolotti FP, Hein S, Simen M, Dallmann U. 1995. Nichtlokale und nichtlineare Instabilitätsuntersuchungen an kompressiblen Strömungen. *DLR IB 223-95 A54*

Stuckert G, Herbert Th. 1993. Nonlinear analysis of swept wing transitional boundary layers. *SAE Pap. No. 932515*

Stuckert G, Herbert Th, Esfahanian V. 1993. Stability and transition on swept wings. *AIAA Pap. No. 93-0078*

Taylor GI. 1938. Some recent developments in the study of turbulence. In *Proc. Int. Congr. Applied Mechanics, Cambridge, Massachusetts*, pp. 294–309

Tollmien W. 1929. Über die Entstehung der Turbulenz. *Nachr. Ges. Wiss. Göttingen, Math.-Phys. Kl.*, pp. 21–44

Trefethen LN, Trefethen AE, Reddy SC, Driscoll TA. 1993. Hydrodynamic stability without eigenvalues. *Science* 261:578–84

Van Ingen JL. 1956. A suggested semi-empirical method for the calculation of the boundary layer transition region. *Dept. Aero-*

naut. Eng., Delft Univ. Tech., Rep. No. VTH 74

Waleffe F. 1995. Hydrodynamic stability and turbulence: beyond transients to a self-sustaining process. *Stud. Appl. Math.* 95: 315

Wang M. 1994. *Stability analysis of three-dimensional boundary layers with parabolized stability equations*. PhD thesis, Ohio State Univ., Columbus

Wang M, Herbert Th, Stuckert GK. 1994. PSE analysis of receptivity and stability in swept wing flows. *AIAA Pap. No. 94-0180*

Wang T, Simon TW, Buddhavarapu J. 1985. An experimental investigation of curvature and freestream turbulence effects on heat transfer and fluid mechanics in transitional boundary layer flows. *NASA Rep. No. NAG 3-286*

Westin K JA, Boiko AV, Klingmann BGB, Kozlov VV, Alfredsson PH. 1994. Experiments in a boundary layer subjected to free stream turbulence. Part I: Boundary layer structure and receptivity. *J. Fluid Mech.* 281:193–218